PCCP

Accepted Manuscript

This is an *Accepted Manuscript*, which has been through the Royal Society of Chemistry peer review process and has been accepted for publication.

Accepted Manuscripts are published online shortly after acceptance, before technical editing, formatting and proof reading. Using this free service, authors can make their results available to the community, in citable form, before we publish the edited article. We will replace this *Accepted Manuscript* with the edited and formatted *Advance Article* as soon as it is available.

You can find more information about *Accepted Manuscripts* in the Information for Authors.

Please note that technical editing may introduce minor changes to the text and/or graphics, which may alter content. The journal's standard Terms & Conditions and the Ethical guidelines still apply. In no event shall the Royal Society of Chemistry be held responsible for any errors or omissions in this *Accepted Manuscript* or any consequences arising from the use of any information it contains.

ROYAL SOCIETY OF CHEMISTRY

www.rsc.org/pccp

DFT+U computational study stoichiometric and oxygen deficient M/CeO_2 systems ($M = Pd_1$, Rh_1, Rh_{10}, Pd_{10} and Rh_4Pd_6)

YongMan Choi[a], M. Scott[c], T. Söhnel[c] and Hicham Idriss[b,d] *

[a] SABIC Technology Center, Riyadh, 11551, Saudi Arabia

[b] SABIC Center for Research and Innovation (CRI) at King Abdullah University of Science of Technology (KAUST), Thuwal, 23955, Saudi Arabia

[c] School of Chemical Sciences, The University of Auckland, Private Bag 92019, Auckland, New Zealand.

[d] Department of Chemistry, University College London, 20 Gordon Street, London WC1H 0AJ, U.K.

*Corresponding author: Tel: +966-12-275-5060;

E-mail: idrissh@SABIC.com and h.idriss@ucl.ac.uk

Physical Chemistry Chemical Physics Accepted Manuscript

TOC (Table of content) image

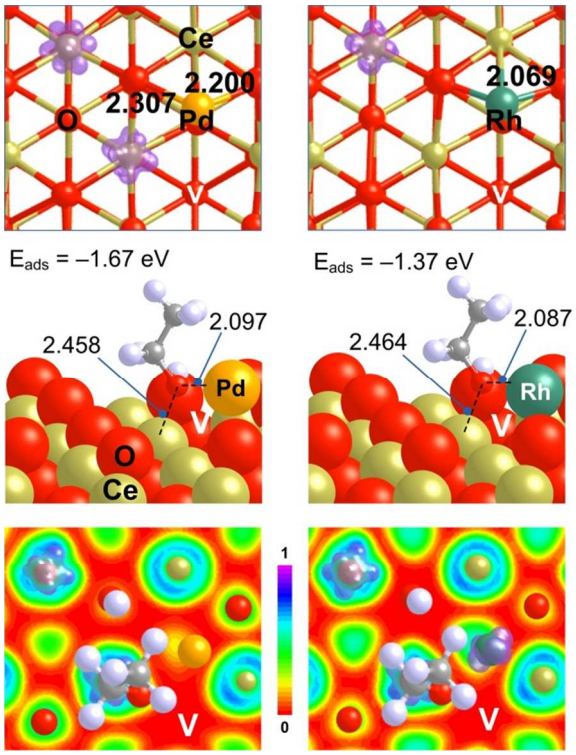

Keywords:

CeO_2(111); Ethanol adsorption; DFT + U; Ce4f DOS; Adsorption energy, Electron transfer, Oxygen vacancy.

Physical Chemistry Chemical Physics Accepted Manuscript

ABSTRACT

Molecular and dissociative adsorption of ethanol on stoichiometric and O-defected CeO_2 (111) surfaces alone as well as in the presence of one metal atom (Pd or Rh) are studied using spin-polarized density functional theory (DFT) with the GGA + U method (U_{eff} = 5.0 eV). Dissociative adsorption (to ethoxides) is slightly more stable than molecular adsorption on stoichiometric CeO_2(111). The creation of surface oxygen vacancies further stabilizes both modes. In the case of ethoxide adsorbed on a Ce^{3+} cation, adjacent to the oxygen vacancy, charge transfer to a nearest Ce^{4+} cation occurs. In addition, the interactions of Pd_1 (or Rh_1), of Pd_{10} (or Rh_{10}) as well as of a bimetal cluster (Rh_4Pd_6) on perfect and O-defected CeO_2(111) surfaces have been studied. From spin density calculations, it was found that the addition of metal changes the oxidation state of Ce^{4+} cations. The magnetic moment neighboring to Rh or Pd induces a charge transfer to Ce^{4+} cations (*i.e.* Ce^{4+} ($4f^0$) that becomes Ce^{3+} ($4f^1$)) and consequently M is oxidized to $Pd^{\delta+}$ (or $Rh^{\delta+}$). Similar to the atomic metal adsorption, Rh_{10} has a stronger adsorption energy on the perfect surface than Pd_{10} (E_{ads} = –6.49 and –5.75 eV, respectively), while that of the Rh_4Pd_6 was in between (E_{ads} = –6.00 eV). The effect of one metal atom on the adsorption of ethanol was also studied. The presence of the metal further stabilized the adsorption energy of ethanol/ethoxide in its bridging configuration. The creation of an oxygen vacancy nearest to the metal resulted in considerable stabilization of ethoxides (E_{ads} = -1.67 eV in the case of Pd) compared to those found on the O-defected CeO_2(111) alone (E_{ads} = -0.85 eV).

Physical Chemistry Chemical Physics Accepted Manuscript

Physical Chemistry Chemical Physics Accepted Manuscript

1. Introduction

Ceria and ceria containing materials are attracting much interest due to their high activity for many catalytic processes including water gas shift reaction and reforming of hydrocarbons [1, 2]. In addition ceria is one of the most active and stable materials for hydrogen production from water via thermal routes due to its high redox activity [3-7]. One of the main reasons for its high activity is the fast oxygen transport making oxidation reactions possible and the ease by which Ce^{4+} is reduced to Ce^{3+} making reduction reactions possible [8]. The performance of these oxidation/reduction cycles of ceria is improved by either the addition of metals [9], mainly in catalysis, or doping with other metal cations [10-12], mainly in thermal reaction such as hydrogn production (a stoichiometric (not a catalytic) process). In the case of pure ceria, the formation of Ce^{3+} cations and the associated oxygen vacancies have been studied in some details experimentally (XPS, TPD, ISS, XAS, and STM among others [13-17]) and by computation methods (at the HF, DFT, MP2 levels [18-27] for both catalytic and energy (hydrogen production) applications. In particular it has been pointed out the lack of priori for the geometric arrangement of the oxygen vacancies unlike what was initially thought [18].

Because many catalytic processes on CeO_2 involve the presence of a metal [17, 28-33], the interface of metal/CeO_2 is crucial for the understanding of surface reactions. For example, in the case of the catalytic hydrogen production via steam reforming of ethanol (an example of biomass), it has been recognized early on that over ceria one can make very active catalysts using a bimetal system where one metal is required for fast hydrogen-hydrogen bond formation (such as Pd [30, 31] and the other carbon-carbon bond dissociation (such as Rh [32] or Ru [17]).

The nature of interaction of metals with oxides can be studied at the atomic [34, 35], electronic [36, 37] and energy (for example, adsorption and interaction energies [38]) levels. Extent of

reduction [31], electron transfer [39] and adsorption energies [40] change considerably with the nature or size of the metals particles and therefore in the case of CeO_2 deserve attention.

In this work, we undertake spin-polarized DFT calculations with the GGA-PBE + U method to study in more details the different interactions of ethanol on perfect and oxygen deficient CeO_2(111) surfaces with and without a noble metal (M = Pd or Rh). Furthermore, we studied the interactions of Pd_{10}, Rh_{10}, and Rh_4Pd_6 clusters on perfect and oxygen deficient CeO_2(111) surfaces in order to probe the nature of interaction of these monometallic and bimetallic clusters with the reducible oxide surface.

2. Computational methods

Spin-polarized DFT calculations were carried out using the Vienna ab initio simulation package (VASP) [41, 42]. In this study, the interaction between core and valence electrons was treated with the projector augmented wave (PAW) method [43], while the exchange-correction interaction was described using the Perdew-Burke-Ernzerhof (PBE) functional [44]. All calculations were carried out with a 415 eV kinetic energy cut-off for a plane wave basis set. Monkhorst-Pack meshes with (3 × 3 × 3) and (4 × 4 × 1) **k**-points were utilized for bulk and surface calculations, respectively. In particular, to accurately describe the strong on-site Coulomb repulsion of the Ce 4f electrons, the PBE + U with an effective U value of 5.0 eV (U_{eff} = 5.0 eV) was used similar to previous studies [23, 45, 46]. Adsorption energies (E_{ads}) were calculated by $E_{ads} = E_{(adsorbate/CeO2)} - E_{(CeO2)} - E_{(adsorbate)}$. $E_{(adsorbate\ /CeO2)}$, $E_{(CeO2)}$, and $E_{(adsorbate)}$ are the calculated energies of an adsorbate on ceria, a bare ceria, and an adsorbate. To avoid interactions between slabs, we used a vacuum space of 15 Å. In addition, the charge analysis was

Physical Chemistry Chemical Physics Accepted Manuscript

carried out using the Bader charge analysis technique [47, 48], while vibrational frequencies were calculated to compare with experimental results [30, 31]. We also calculated the electron localization function (ELF) on the basis of optimized structures [49, 50]. We have also conducted in the case of ethanol adsorption on CeO_2(111) DFT+U including dispersive interaction using a variety of functionals: revPBE-vdW+U, vdW-DF2+U, optB86b-vdW+U, optPBE-vdW+U, and optB88-vdW+U [24].

3. Results and Discussions

3.1. Validity of surface models

The calculated lattice constant of bulk CeO_2 of 5.45 Å at the PBE + U method is in good agreement with the experimental and other theoretical values [22, 51] of 5.411 Å and 5.48 Å, respectively, Figure 1a. Shown in Figure 1b is the projected density of states (PDOS) for bulk CeO_2 with U_{eff} = 5.0 eV. The computed energy gaps of O 2p → Ce 4f and O 2p → Ce 5d depends on the functional used with a general overestimation with the inclusion of HF in hybrid functionals and underestimation with LDA, PBE and PW91. In this work the values obtained are 2.25 eV and 5.31 eV, for O 2p → Ce4f and O 2p → Ce5d, respectively [52]. Both changes in lattice constant and energy gaps with the use of different functionals and computation methods are given in Table 1. Surface energies of CeO_2(100), (110), and (111) are given (Figure 1c) in units of J/m^2, according to E_{surf} = 1/2S (E_{slab} – E_{bulk}) where S, E_{slab}, and E_{bulk} are the surface area of each plane, and the calculated energies of the slab and the bulk, respectively.

As summarized in the Table inside Figure 1, the computed relaxed surface energies are lower than those of the un-relaxed surfaces as seen previously on this system by other workers [53]; which is common to ionic systems in general. It is also consistent with experiments where the (111) surface of CeO_2 (and the fluorite structure in general) is the most stable [54]. To further

Physical Chemistry Chemical Physics Accepted Manuscript

verify the surface model using the PBE + U method, we have calculated H_2O adsorption energies on CeO_2 (111) since its experimental data is available in the literature. As shown in Figure S1, we found that the configuration in which the oxygen of H_2O is in interaction with Ce^{4+} cations and one of its H atoms is in interaction with surface O anions (H-$\mathbf{O_s}$ bond = 1.634 Å and its adsorption energy is = –0.45 eV) is in good agreement with experimental results (–0.51 ~ –0.61 eV) [55]. The table inside Figure S1 gives a summary of adsorption energies on CeO_2 by others. The configurations of the perfect and defective surfaces for p(2 × 2) CeO_2(111) are shown in Figure 2a,b,c, and their PDOS is displayed in Figure 2d,e. Similar to the bulk structure, the valance band on the perfect surface consists of O 2p, while the conduction band mainly arises from Ce 5d, including a narrow, unoccupied band of Ce 4f. However, the defective surface has an occupied band near the Fermi level (Ce 4f). Also shown is the PDOS plot of Ce 4f from Ce^{3+} and Ce^{4+} on the defective CeO_2(111) surface. In addition, it was found that the spin is highly localized on the two Ce ions near the oxygen vacancy (Figure 2c) [56].

3.2. Adsorption of ethanol and ethoxide on perfect and defective CeO_2 (111)

For surface calculations, half of the atomic layers of the 12-layer slab is fixed to the bulk structure, the remaining layers and the adsorbate were fully relaxed. Shown in Figure 3 is the adsorption of ethanol on perfect CeO_2(111) surface. Table 2 compiles the geometric parameters (Figures 3a and 3b) and adsorption energies of ethanol in its molecular and dissociated modes (ethoxides). Computation conducted without the inclusion of dispersive interaction indicated that a configuration vertical to the surface to be slightly more stable than that parallel to the surface from 0.25 to 1.0 ML, where 1 ML is defined with respect to the Ce^{4+} cation; no stable adsorption was found for the molecular adsorption at 1 ML. The small difference of about 0.1

Physical Chemistry Chemical Physics Accepted Manuscript

eV can be seen as due to repulsive interaction between the carbon atoms and surface oxygen atoms that may offset any gain due to secondary interaction between the H atoms of the terminal carbon and surface oxygen. Similar results were seen on TiO_2(110) [57]. The trend is not changed for the ethoxide modes (Figure 4), although they have (in both configurations) slightly stronger adsorption energies than ethanol (the corresponding vibrational frequencies are given in Table 3). In order to further check the different stabilities of ethanol and ethoxides in their minimized geometry we have computed the adsorption energy including van der Waals (vdW) interaction. We have included vdW interaction to gauge the effect of secondary interaction between H atoms of ethanol/ethoxides with surface oxygen atoms. We have in particular observed that the omission of this interaction made the ethoxide orientation perpendicular to the surface to be more stable than that parallel yet its inclusion resulted in an iso-energetic system. Tables S1, S2 and S3 present the results with different exchange-correlation functionals. As can be seen the inclusion of vdW resulted in decreasing the slight energy difference between the parallel and vertical modes of both ethanol and ethoxides. The difference in both configurations decreased to almost zero eV from up to 0.12 eV suggesting that both modes have similar stabilities on this oxygen terminated surface.

The partially filled electronic states created upon the removal of the surface oxygen anions may further stabilize/destabilize the adsorbates. As shown in Figure 5, molecular and dissociative adsorptions of ethanol and ethoxide have a stronger energy on the defective surface when compared to the perfect surface. Evidence of charge transfer are seen in the dissociated mode, the Ce^{3+} ion became the Ce^{4+} ion, resulting in one electron donation to a neighboring Ce^{4+} ion (Figure 5f). Accordingly, the local magnetic moment of the Ce atom in the unit of μB is changed

Physical Chemistry Chemical Physics Accepted Manuscript

from 0.959 to 0.007. In addition, due to a surface reconstruction after generation of oxygen vacancies, the average Ce-O bond distance of the topmost trilayer is shortened (2.363 Å vs. 2.358 Å), while the topmost oxygen layer moves upward (~1.1%). These electronic and structural changes may be reasons why ethanol is more stabilized on the defective surface.

Figure 6 shows DOS plots of molecularly and dissociatively adsorbed ethanol on perfect and defective CeO_2(111), while Figure 7 presents the pDOS on Ce and O involved in the bonding. The effect on the change of adsorption types (molecular versus dissociative adsorption) is not significant. Similar to the bare defective surface (Figure 2d), partially filled Ce 4f orbitals are still observed on the defective surfaces. From examination of the molecular adsorption on defective CeO_2(111), it is found that O 2p orbitals of ethanol and Ce^{3+} have interacted (Figure 7c).

3.3. Pd and Rh on perfect and defective CeO_2 (111)

As shown in Figure 8 a, d, similar to a previous study [23], Rh preferentially occupies the hollow sites, while Pd occupies the bridge site. Rh is more strongly bound to the surface when compared to Pd (–3.70 eV vs. –1.79 eV, respectively) yet with a slightly longer M-O distance (2.156 Å vs. 2.12 Å, respectively). In addition, it donates more electrons to the surface (Q_{Rh} = +0.63e vs. Q_{Pd} = +0.34e) in line with their ionization potential. In other words, Rh is energetically more stable on CeO_2 (111) as compared to Pd.

From spin density calculations, it was found that the addition of metal changes the oxidation state of Ce atoms. The magnetic moment neighboring to Rh or Pd induces a charge transfer to Ce^{4+} cations (*i.e.* Ce^{4+} ($4f^0$, non-magnetic) that becomes Ce^{3+} ($4f^1$, magnetic) [23]) and consequently M is oxidized in $Rh^{\delta+}$ or $Pd^{\delta+}$. Figure 8 shows that the net spin densities are

Physical Chemistry Chemical Physics Accepted Manuscript

localized on the metal adatoms and the neighboring Ce^{3+}. This is similar to what has been computed for both metals on stoichiometric $CeO_2(111)$[5]. In addition, as shown in Figure S2, $M/CeO_2(111)$ surfaces show new additional peaks due to Pd and Rh orbitals. The DOS results indicate that M d states overlap with O 2p states near the Fermi energy.

In order to see the effect of the presence of M on adsorption ethanol was introduced in a bidentate configuration in which the oxygen atom of ethanol/ethoxide are bonded to Ce cations as well as to the Rh (or Pd) metal, Figure 8b,c,e. Within this bidentate configuration (at 0.25 ML), ethanol on Rh/CeO_2 (111) is only dissociatively adsorbed (–0.34 eV), while on Pd/CeO_2 (111) both molecular and dissociative modes were found to be stable (and almost isoenergetic) (–0.73 eV versus –0.67 eV, respectively). Figure S2 shows the overlap of ethanol O 2p with M 4d orbitals, evidence of interaction. Similar interaction occurs with Ce 4f (Figure S3).

Furthermore, we examined the metal adatom effect on the interaction of ethanol on a defective surface (Figure 9). Compared to the perfect surface, the adsorption energy of Rh on the defective surface is slightly weaker (–3.37 eV), while that of Pd remains the same (–1.79 eV). The oxygen vacancy affects the average M-O distances (2.087 Å vs. 2.254 Å, respectively) compared to those on the perfect ones (2.156 Å vs. 2.122 Å, respectively). The trend of electron transfer is the same as on the perfect surface (Q_{Rh} = +0.17e vs. Q_{Pd} = +0.03e) albeit much weaker; which is simply understood as due to decrease in charge transfer because the defective surface is already charged. Interestingly, while the $Pd/CeO_2(111)$ surface still has two localized Ce^{3+} ions, $Rh/CeO_2(111)$ has only one (Figure 9). DOS calculations also show that more Ce^{3+} states (Ce4f) are available on $Pd/CeO_2(111)$ than on $Rh/CeO_2(111)$ (Figure S4). For the ethanol adsorption, it is fully dissociated to C_2H_5O + H, resulting in O-H distance of 2.893 Å and 2.796 Å on $Rh/CeO_2(111)$ and $Pd/CeO_2(111)$, respectively. Similar to the dissociative adsorption on the

Physical Chemistry Chemical Physics Accepted Manuscript

perfect surface, ethoxides on $Pd/CeO_2(111)$ are more stable compared to those on $Rh/CeO_2(111)$ (E_{ads} = –1.67 eV vs. –1.37 eV, respectively). Upon dissociative adsorption on $Rh/CeO_2(111)$, evidence of charge transfer can be seen for the Ce ion linked to the C_2H_5O in addition to spin localization on the Rh adatom. Also as in the case of the perfect surface O 2p and Ce 4f are highly overlapping (Figure S5).

3.4. Adsorption of Pd_{10}, Rh_{10}, and Rh_4Pd_6 nanoclusters on perfect and defective CeO_2 (111).

In order to further probe into the role of metal atoms interaction with the surfaces of CeO_2 we have studied the adsorption of M_{10} cluster of atoms on the (111) surface. Pd_{10}, Rh_{10}, and Rh_4Pd_6 nanoclusters on perfect and defective $CeO_2(111)$ were computed. Initially, to choose a realistic proto-type of nanoclusters, we followed a previous study by Zhang et al. [58]. The binding energy (BE) per atom is calculated by $[E_{(M\ atom)} \times N - E_{(NC)}]/N$, where $E_{(M\ atom)}$ and $E_{(NC)}$ are the calculated electronic energies of an M atom and a nanocluster (NC), respectively. Also, N is the number of atoms in the nanoclusters. In addition, we compared the relative energies (E_{rel}) of each nanocluster relative to the most stable one according to $E_{rel} = E_{(NC's\ electronic\ energy)} - E_{(NC\ with\ the\ lowest\ electronic\ energy)}$.

As compiled in Table 4, it was found that the tetrahedral M_{10} structure of both Pd and Rh has a slightly stronger binding energy compared to other models with the shortest M-M bond length. Thus we chose the tetrahedral structure for the examination of the interaction of M_{10} on $CeO_2(111)$. In addition, as shown in the inset of Figure 10, it was reported that $Rh_{0.5}Pd_{0.5}/CeO_2$ catalysts were the most active toward ethanol reforming, among different Rh/Pd ratios [32]. Thus, we have also created bimetallic Rh_xPd_y nanoclusters. As shown in Figure 10, we found that as Rh is mixed with Pd, it becomes more stabilized. To keep the symmetry simple of the surface

Physical Chemistry Chemical Physics Accepted Manuscript

adsorbate model, the bottom Pd atoms were equilaterally linked to the CeO_2 surface oxygen atoms; therefore, we have opted for the Rh_4Pd_6 nanocluster. A more symmetric Rh_4Pd_6 configuration (C_{3V}), in which Rh sits at each vertex and has a slightly higher BE than the clustered one (–1.99 eV vs. –1.83 eV, respectively) chosen for the adsorption calculations together with pure Rh_{10} and Pd_{10}. As summarized in Table S5, while the atoms at vertex are negatively charged, spin density calculations show that Rh in the Rh_4Pd_6 nanocluster has more spin compared to Rh_{10} (Figure S6).

On perfect CeO_2(111) surface, as shown in Figure 11, the Rh nanocluster is more strongly bound to the surface than Pd (per cluster: –6.49 eV vs. –5.75 eV, respectively and per atom: -4.45 eV vs. -2.69 eV, respectively), while the averaged O-M bond distances are comparable (2.074 eV vs. 2.019 eV, respectively). The trend in adsorption energy is similar to the atomic Pd and Rh adsorption. The trend of charge transfer from the metal cluster to the surface is also the same as that on the atomic Rh and Pd adsorptions ($Q_{Rh} > Q_{Pd}$). The bimetallic Rh_4Pd_6 nanocluster donates slightly less charge to the surface than Pd_{10} and Rh_{10} (1.02e vs. 1.20 and 1.21e, respectively). Furthermore, we found that the creation of an oxygen vacancy at the center, between the vertices, leads to a slightly stronger adsorption of nanoclusters than the perfect M/CeO_2(111) surface.

The spin density analyses on the perfect CeO_2(111) shows that due to the metal nanocluster adsorption, one electron is localized on one Ce 4f ion in the case of Rh_4Pd_6 and two electrons are localized on two Ce 4f ions in the case Rh_{10} (Figure 11 b and c); the Pd_{10} cluster does not generate any localized Ce^{3+} ion (similar to the case of one Pd atom). Some spin is also located on the nanoscluster, especially on Rh_{10} (Figure 11 c). After the creation of an oxygen vacancy, Pd_{10} nanocluster still does not generate any Ce^{3+}, while Rh_4Pd_6 and Rh_{10} have one additional Ce^{3+} ion

Physical Chemistry Chemical Physics Accepted Manuscript

(Figure 11). In the case of the Pd_{10} cluster, the generation of the oxygen vacancy results in charge transfer from CeO_2(111) to the cluster based on the change of spin density (Figure 11d).

4. Discussion

From the above study the following observations can be made.

1. Ethanol adsorption is slightly more favored in its dissociative mode compared to the molecular mode on perfect CeO_2(111) (tables 1 and 2) and defective CeO_2(111) surfaces. The adsorption energies of ethanol and ethoxides decrease with increasing surface coverage from 0.25 to 1 ML.
2. The creation of oxygen vacancies increases the adsorption energy of ethanol/ethoxide (from ca. 0.4 eV on the stoichiometric surface to ca. 0.8 eV on the oxygen defective surface). In the ethoxide adsorption mode, on oxygen defective CeO_2(111), charge transfer occurs from one Ce^{3+} cation (on which ethoxide is bound) to a next neighbor Ce^{4+} cation. Molecular adsorption does not create this charge transfer.
3. Charge transfer from one atom of Rh or Pd to CeO_2(111) occurs; with Rh donating more charges than Pd (Q_{Rh} = +0.63e vs. Q_{Pd} = +0.34e).
4. Ethanol adsorption in a bidentate configuration on M/CeO_2 results in molecular and dissociative adsorption modes in the case of Pd while only a dissociative mode was seen in the case of Rh. Upon the creation of one oxygen vacancy two localized Ce 4f are seen in the case of Pd and only one in the case of Rh.

Physical Chemistry Chemical Physics Accepted Manuscript

5. Adsorption of ethanol only leads to ethoxides on Rh or Pd/CeO_2 (111) in presence of one oxygen vacancy. Charge transfer as in point 2 is only seen for the Rh/defective CeO_2(111).
6. Rh_{10} and Pd_{10} clusters deposited on CeO_2(111) show similar trend in adsorption energy and charge transfer to those of one metal of Rh or Pd.
7. Charge transfer is seen to occur in the Rh_{10} and Rh_4Pd_4 creating one Ce^{3+} cation. The creation of an oxygen vacancy on the surface located at the center between the vertices of the Rh_{10} or Rh_4Pd_6 clusters results in the formation of a total of three Ce^{3+} cations.

Molecular versus dissociative adsorption modes is mainly governed by what is termed "proximity effect" and the strength of the degree of ionicity of the surface oxygen atoms. Because the interaction occurs between the O2p orbitals of ethanol and Ce^{4+} cations in the second layer the hydrogen of the hydroxyl group is in close proximity to the surface oxygen (last layer) making its dissociation possible but also allowing for considerable hydrogen bonding because of the three-fold symmetry and the short distance O_l-Ce^{4+} distance. Figure 5 shows that both structures are very similar with the main difference being the closer O_a-Ce^{4+} distance in the case of ethoxide, where *a* stands for adsorbate. DFT (PW91 + U) computation of methanol adsorption over CeO_2(111) was conducted by other workers [59], it was also observed that the adsorption energy is increased when methanol/methoxide is adsorbed on top of the oxygen vacancy triply- as well as doubly-bridged to the Ce cations. Experimentally the adsorption and reaction of a series of alcohols has been studied on stoichiometric and oxygen deficient CeO_2(111) thin layer by TPD and XPS [60]; although based on XPS C1s it was proposed that alkoxides are formed no STM study so far has probed into the ethanol/ethoxide modes of

Physical Chemistry Chemical Physics Accepted Manuscript

adsorption. IR studies has shown that indeed ethanol is present along with ethoxides based on the banding mode of δOH at 1265 cm^{-1} and δ_{as} CH_3 [28, 29] attributed to molecularly adsorbed ethanol on powder CeO_2 with and without a metal. Other works have also addressed the adsorption and reaction of methanol on CeO_2(111) grown on Cu(111) [15]. It was observed that the three types of methoxides (monodentate, bidentate and tridentate) are formed on a thick layer of CeO_2(111) (over 10 ML) as in the case of CeO_2 powder. However on a thin layer of CeO_2(111) (3 ML) methoxides are mainly in bi- and tri-dentate modes). These results together with those of Ce3d XPS, suggesting the presence of surface oxygen vacancies on the thin layer, are in line with the preferential dissociative adsorption on oxygen vacancies. Another work has addressed the same reaction also using core level spectroscopy and found a continuous shift of the XPS C1s of the C-OH group with increasing annealing temperature indicative of dissociation to C-O (from 287.7 eV at 110K to 286.3 eV at 400K [15]; it is to be noted that at 300K (where all multilayers have desorbed) both molecular and dissociative forms are present.

The addition of metals to CeO_2 modifies the adsorption modes and energetics. In this work it was found that the adsorption energy for ethanol on stoichiometric CeO_2(111) is increased in presence of one Pd atom but stayed about the same for Rh. Given that a larger charge transfer occurred from Rh to CeO_2(111) compared to Pd the results can be rationalized by the fact that Rh is mainly present as an Rh cation while Pd still contain larger fraction of d electrons to increase the adsorption via hybridization. Experimental work [61] of methanol adsorption over Pt/CeO_2(111) also indicated a farther stabilization of methanol/methoxides compared to CeO_2(111) alone. The creation of oxygen vacancies (this work) resulted in considerable increase of the adsorption energy of ethanol (with only dissociative mode observed) yet the effect of both metals was comparable (1.67 eV for Pd/CeO_2(111) and 1.37 eV for Rh/CeO_2(111) higher that the

Physical Chemistry Chemical Physics Accepted Manuscript

0.85 eV in the absence of the metal). Another DFT + U computation work over 4Rh/CeO_2(111) has also indicated that ethanol is dissociatively adsorbed in the interface leading to stable ethoxide species (E_a = 2.5 eV) [62].

Evidence of charge transfer can be seen in figures 8 and 9 for both metals (Rh and Pd). This is in line with experimental and computational results for Pd on CeO_2(111); grown on Pt(111) [14] where the authors found charge transfer to be localized on the 4f orbitals of one Ce atom as in this work. A compilation of the different metal clusters studied by computational methods over CeO_2(111) is given in table 5 together with the charge transfer in units of e. Highest adsorption energy is found for Rh and lowest for Au which is to a first approximation also in line with the charge transfer because of the high ionic character of oxygen ions of CeO_2(111) surfaces.

5. Conclusions

Surface models of CeO_2(111) in its perfect and oxygen defective states, using the GGA-PBE + U method (U_{eff} = 5.0 eV) were obtained by studying various properties, such as band gap and H_2O adsorption. The creation of an O vacancy enhances the adsorption of ethanol and ethoxide on CeO_2(111). It was found that Rh has a far stronger adsorption energy on the perfect surface than Pd (–3.70 and –1.79 eV). The dissociatively adsorbed ethanol is more strongly bound on both perfect and defective Pd/CeO_2 than Rh/CeO_2 (–0.67 and –0.34 eV on the perfect surface; –1.67 and –1.37 eV on the defective surface, respectively). Nanoclusters of 10 metals atoms were studied in the gas phase and on CeO_2(111) surface. Rh_{10} has a stronger adsorption energy on the perfect surface than Pd_{10} (–6.49 and –5.75 eV, respectively), while such energy in bimetallic systems depends upon their ratio of Rh and Pd (Rh_4Pd_6: E_{ads} = –6.00 eV). The formation of an oxygen vacancy affects the binding energy of Pd_{10}, Rh_4Pd_6 and Rh_{10} (–6.02, –6.19, and –6.66 eV, respectively). DOS calculations show that the metal-O binding results in hybridization of the

Physical Chemistry Chemical Physics Accepted Manuscript

metal d orbitals and surface O 2p. Bader charge analysis has shown that the charge transfer occurs from the clusters to ceria.

Acknowledgements

DFT calculations were performed at the National Energy Research Scientific Computing (NERSC) Center (Contract No. DE-AC02-05CH1231) and partially at KAUST Supercomputing Laboratory (KSL). Y.C. thanks Dr. Zhengji Zhao at NERSC and Dr. Dodi Heryadi and Mr. Andrew C. Winfer at KSL for the technical support for DFT calculations.

References

[1] J.A. Rodriguez, P. Liu, J. Hrbek, J. Evans, M. Pérez, Angew. Chem. Int. Ed., 46 (2007) 1329-1332.
[2] J.A. Rodriguez, J. Graciani, J. Evans, J.B. Park, F. Yang, D. Stacchiola, S.D. Senanayake, S. Ma, M. Pérez, P. Liu, J.F. Sanz, J. Hrbek, Angew. Chem. Int. Ed., 121 (2009) 8191-8194.
[3] W.C. Chueh, F. C., A. M., S. D., F. P., H.S. M., A. Steinfeld, Science, 330 (2010) 1797-1801.
[4] I.I. Al-Shankiti, F. Al-Otaibi, Y. Al-Salik, H. Idriss, Top Catal., 56 (2013) 1129–1138.
[5] Y. Al-Salik, I. Al-Shankiti, H. Idriss, Core level spectroscopy of oxidized and reduced $Ce_xU_{1-x}O_2$ materials, (2013) in press, http://dx.doi.org/10.1016/j.elspec.2013.1011.1013.
[6] Y. Al-Salik, H. Idriss, Syngas (CO and H_2) Production from H_2O and CO_2 over CeO_2 Materials Doped with Fe and U Metal Cations, US Patent application. Project Number 13T&I0075, 2013.
[7] M. Roeb, M. Neises, N. Monnerie, F. Call, H. Simon, C. Sattler, M. Schmücker, R. Pitz-Paal, Materials, 5 (2012) 2015-2054.
[8] P.P. Dholabhai, J.B. Adams, P. Crozier, R. Sharma, J. Chem. Phys. 132 (2010) 094104.
[9] Z. Yang, G. Luo, Z. Lu, K. Hermansson, J. Chem. Phys. 127 (2007) 074704.
[10] H. Kaneko, T. Miura, H. Ishihara, S. Taku, T. Yokoyama, H. Nakajima, Y. Tamaura, Energy, 32 (2007) 656-663.
[11] S. Abanades, A. Legal, A. Cordier, G. Peraudeau, G. Flamant, A. Julbe, J. Mater. Sci., 45 (2010) 4163-4173.
[12] Y. Tang, H. Zhang, L. Cui, C. Ouyang, S. Shi, W. Tang, H. Li, J.-S. Lee, L. Chen, Phys. Rev. B 82 (2010) 125104.
[13] M.A. Henderson, C.L. Perkins, M.H. Engelhard, S. Thevuthasan, C.H.F. Peden, Surf. Sci. 526 (2003) 1-18.

Physical Chemistry Chemical Physics Accepted Manuscript

[14] E.L. Wilson, R. Grau-Crespo, C.L. Pang, G. Cabailh, Q. Chen, J.A. Purton, C.R.A. Catlow, W.A. Brown, N.H. de Leeuw, G. Thornton, J. Phys. Chem. C 112 (2008) 10918-10922.
[15] V. Matolín, J. Libra, M. Škoda, N. Tsud, K.C. Prince, T. Skála, Surf. Sci. 603 (2009) 1087-1092.
[16] D. Kong, G. Wang, Y. Pan, S. Hu, J. Hou, H. Pan, C.T. Campbell, J. Zhu, J. Phys. Chem. C 115 (2011) 6715-6725.
[17] W. Xu, R. Si, S.D. Senanayake, J. Llorca, H. Idriss, D. Stacchiola, J.C. Hanson, J.A. Rodriguez, J. Catal. 291 (2012) 117-126.
[18] F. Esch, S. Fabris, L. Zhou, T. Montini, C. Africh, P. Fornasiero, G. Comelli, R. Rosei, Science 309 (2005) 752-755.
[19] B. Herschend, M. Baudin, K. Hermansson, Surf. Sci. 599 (2005) 173-186.
[20] M. Fronzi, A. Soon, B. Delley, E. Traversa, C. Stampfl, J. Chem. Phys. 131 (2009) 104701-1 to 104701- 16.
[21] H.-Y. Li, H.-F. Wang, X.-Q. Gong, Y.-L. Guo, Y. Guo, G. Lu, P. Hu, Phys. Rev. B 79 (2009) 193401-1 to 193401-4.
[22] J.S. Graciani, A.M. Márquez, J.J. Plata, Y. Ortega, N.C. Hernández, A. Meyer, C.M. Zicovich-Wilson, J.F. Sanz, J. Chem. Theor. Comp. 7 (2010) 56-65.
[23] Z. Lu, Z. Yang, J. Phys. Condens. Matter. 22 (2010) 475003.
[24] D. Fernández-Torre, K. Kośmider, J. Carrasco, M.V. Ganduglia-Pirovano, R. Pérez, J. Phys. Chem. C, 116 (2012) 13584-13593.
[25] D. Mei, Q. Ge, Comput. Theor. Chem., 987 (2012) 25-31.
[26] M. Aryanpour, A. Khetan, H. Pitsch, ACS Catal., 3 (2013) 1253-1262.
[27] J. Kullgren, M.J. Wolf, C.W.M. Castleton, P. Mitev, W.J. Briels, K. Hermansson, Phys. Rev. Lett., 112 (2014) 156102-1 to 156102-5.
[28] P.Y. Sheng, A. Yee, G.A. Bowmaker, H. Idriss, J. Catal., 208 (2002) 393-403.
[29] P.Y. Sheng, G.A. Bowmaker, H. Idriss, Appl. Catal. A, 261 (2004) 171-181.
[30] A. Yee, S.J. Morrison, H. Idriss, J. Catal., 186 (1999) 279.
[31] H. Idriss, Platinum Met. Rev., 48 (2004) 105-115.
[32] H. Idriss, M. Scott, J. Llorca, S.C. Chan, W. Chiu, P.-Y. Sheng, A. Yee, M.A. Blackford, S.J. Pas, A.J. Hill, F.M. Alamgir, R. Rettew, C. Petersburg, S.D. Senanayake, M.A. Barteau, ChemSusChem, 1 (2008) 905-910.
[33] A. Bruix, A. Migani, G.N. Vayssilov, K.M. Neyman, J. Libuda, F. Illas, Phys. Chem. Chem. Phys., 13 (2011) 11384-11392.
[34] J.B. Park, J.S. Ratliff, S. Ma, D.A. Chen, Surf. Sci. Reports, 600 (2006) 2913-2923.
[35] M.P. Felicissimo, O.N. Martyanov, T. Risse, H.-J. Freund, Surf. Sci., 601 (2007) 2105-2116.
[36] S. Bashir, A.K. Wahab, D. Anjum, H. Idriss, Appl. Pet. Chem. Res., DOI 10.1007/s13203-014-0051-4
[37] F. Pesty, H.-P. Steinrück, T.E. Madey, Surf. Sci., 339 (1995) 83-95.
[38] S. Kundu, A.B. Vidal, A. Nadeem, S.D. Senanayake, H. Idriss, P. Liu, J.A. Rodriguez, D. Stacchiola, J. Phys. Chem. C, 117 (2013) 11149–11158.
[39] P.V. Kamat, J. Phys. Chem. C, 111 (2007) 2834-2860.
[40] D.C. Meier, D.W. Goodman, J. Am. Chem. Soc., 126 (2004) 1892-1899.
[41] G. Kresse, J. Hafner, Phys. Rev. B, 47 (1993) 558-561.
[42] G. Kresse, J. Furthmuller, Phys. Rev. B, 54 (1996) 11169-11186.
[43] P.E. Blöchl, Phys. Rev. B, 50 (1994) 17953-17979.
[44] J.P. Perdew, K. Burke, M. Ernzerhof, Phys. Rev. Lett., 77 (1996) 3865-3868.

Physical Chemistry Chemical Physics Accepted Manuscript

[45] M. Nolan, S. Grigoleit, D.C. Sayle, S.C. Parker, G.W. Watson, Surf. Sci., 576 (2005) 217-229.
[46] M. Nolan, S.C. Parker, G.W. Watson, Surf. Sci., 595 (2005) 223-232.
[47] R.F.W. Bader, P.M. Beddall, J. Chem. Phys., 56 (1972) 3320.
[48] G. Henkelman, A. Arnaldsson, H. Jonsson, Comput. Mater. Sci., 36 (2006) 354.
[49] A.D. Becke, K.E. Edgecombe, J. Chem. Phys., 92 (1990) 5397.
[50] A. Savin, O. Jepsen, J. Flad, O.K. Andersen, H. Preuss, H.G. von Schnering, Angew. Chem. Int. Ed., 31 (1992) 187.
[51] E.A. Kummerle, G.J. Heger, Solid State Chem., 148 (1999) 485-500
[52] Y. Jiang, J.B. Adams, M.V. Schilfgaarde, J. Chem. Phys., 123 (2005) 064701.
[53] Z. Yang, T.K. Woo, M. Baudin, K.J. Hermansson, J. Chem. Phys., 120 (2004) 7741.
[54] D.M. Lyons, J.P. McGrath, M.A. Morris, J. Phys. Chem. B, 107 (2003) 4607.
[55] M. Prin, M. Pijolat, M. Soustelle, O. Touret, Thermochim. Acta 186 (1991) 273.
[56] N.V. Skorodumova, S.I. Simak, B.I. Lundqvist, I.A. Abrikosov, B. Johansson, Phys. Rev. Lett., 89 (2002) 16601.
[57] J.N. Muir, Y. Choi, H. Idriss, Phys. Chem. Chem. Phys., 14 (2012) 11910-11919.
[58] W. Zhang, Q. Ge, L. Wang, J. Chem. Phys., 118 (2003) 5793-5801..
[59] A. Beste, D.R. Mullins, S.H. Overbury, R.J. Harrison, Surf. Sci., 602 (2008) 162-175.
[60] D.R. Mullins, S.D. Senanayake, T.L. Chen, J. Phys. Chem. C, 114 (2010) 17112-17119.
[61] V. Matolín, V. Johánek, M. Škoda, N. Tsud, K.C. Prince, T. Skála, I. Matolínová, Langmuir, 26 (2010) 13333-13341.
[62] H.-J. Li, H.-L. Chen, S.-F. Peng, J.-J. Ho, Chem. Phys., 359 (2009) 141-150.
[63] M.A.M. Branda, N.C. Hernández, J.F. Sanz, F. Illas, J. Phys. Chem. C, 114 (2010) 1934-1941.
[64] A.D. Mayernick, M.J. Janik, J. Chem. Phys., 131 (2009) 084701-1 to 084701-12.
[65] B.-T. Teng, F.-M. Wu, X.-D. Wen, L.-H. Zhao, M.-F. Luo, ChemPhysChem, 13 (2012) 1261-1271.
[66] Y. Zhao, B. Teng, Z. Yang, Y. Zhao, L. Zhao, M. Luo, J. Phys. Chem. C, 115 (2011) 16461-16466.
[67] H.-T. Chen, Y. Choi, M. Liu, M.C. Lin, ChemPhysChem, 8 (2006) 849.
[68] N.V. Skorodumova, M. Baudin, K. Hermansson, Phys. Rev. B. 69 (2004) 075401.
[69] J. L. F. Da Silva, M. V. Ganduglia-Pirovano, J. Sauer, V. Bayer, G. Kresse, Phys. Rev. B 75 (2007) 045121-1 to 045121-10.

Physical Chemistry Chemical Physics Accepted Manuscript

Physical Chemistry Chemical Physics Accepted Manuscript

Tables and Figures

Table 1. Lattice parameter (a in Å) and energy gap (in eV) for CeO_2 computed using the indicated methods.

Method	a (Å)	O2p-Ce4f (eV)	O2p-Ce5d (eV)	Ref
B3LYP	5.47	3.70	8.16	a
PBE0	5.40	4.30	8.52	a
B1-WC	5.38	3.18	7.48	a
PW91	5.48			b
PBE		2.0	5.64	c
GGA + U (5 eV)	5.45	2.25	5.31	This work
Experiment	5.411			d

[a]Ref. [22]. [b]Ref. [52]. [c]Ref. [69]. [d]Ref. [51].

Table 2. Geometrical parameters and adsorption energies of ethanol and ethoxide on $CeO_2(111)$ from θ = 0.25 to 1.0 ML.

θ (ML)	Ethanol				ethoxide	
	$d_{Ce\text{-}O,\mathbf{M}}$ (Å)	$d_{H\text{-}O,\mathbf{Ce}}$ (Å)	$d_{O\text{-}H}$ (Å)	E_{ads} (eV)	$d_{Ce\text{-}O,\mathbf{M}}$ (Å)	E_{ads} (eV)
0.25	2.595	1.600	1.016	–0.47	2.418	–0.55
0.50	2.641	1.626	1.013	–0.40	2.474	–0.46
1.00	2.659	1.610	1.018	–0.23	2.488	–0.39

Table 3. Comparison of computed vibrational frequencies with experimental of adsorbed ethanol and ethoxide on the perfect and defective $CeO_2(111)$ surfaces at θ = 0.25 ML.

Mode	perfect surface			defective surface		
	C_2H_5OH	C_2H_5O	Expt.	C_2H_5OH	C_2H_5O	Expt.
CH_3 asym.	3050	3056	2960	3062	3054	2963
CH_2 asym.	3020	2858	-	2992	-	-
CH_3 sym.	3001	3041	2836	3013	-	-
CH_2 sym.	2884	2877	-	-	-	-
OC stretching	1049	1033	1057 1107	1047	1029	1058 1104

[a] From Ref. [30].

Table 4. Binding energies (BE), relative energies (E_{rel}), and their metal-metal distances of gas-phase Pd_{10} and Rh_{10} nanoclusters.

M_{10}	M	d_{M-M} (Å)	BE (eV/atom)	E_{rel} (eV)
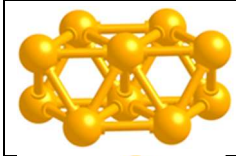	Pd	2.684	–1.54	0.00
	Rh	2.594	–2.14	0.28
	Pd	2.683	–1.58	0.46
	Rh	2.559	–2.11	0.00
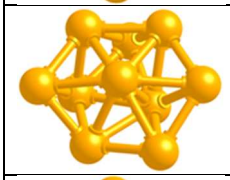	Pd	2.686	–1.56	0.23
	Rh	2.582	–2.17	0.59
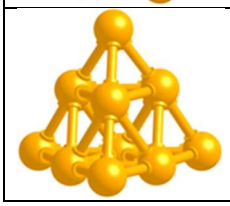	Pd	2.659	–1.60	0.59
	Rh	2.540	–2.24	1.24

Physical Chemistry Chemical Physics Accepted Manuscript

Table 5. Adsorption energy (eV), Bader charge (e) for one metal atom deposition on CeO_2(111) surfaces. Also shown are results for 10 atoms clusters of Au, Pd, Rh and PdRh.

Element	E_{ads} (eV)	Q (e)	References
Cu	1.86 h	0.7	b
Ag	1.0 h	0.56	b
Au	0.71 t	≈ 0	b
Pd	1.78 b	0.48	c
Pd	1.78 h		d
Pd	1.49 t		d
Pt	2.91 b	0.48	c
Rh	3.72 h	0.61	c
Au	1.08 t		e
Au	0.91 h		e
Au_{10}	2.55 per atom		e
Au_{10} *R*	2.58 per atom		e
Sn	2.4 t		f
Sn	3.68 h		f
Pd	1.79 b	0.34	This work
Rh	3.70 h	0.63	This work
Pd_{10}	5.75 (2.69 per atom)	1.20	This work
Pd_{10} *R*	6.02 (2.72 per atom)	1.20	This work
Rh_{10}	6.49 (4.40 per atom)	1.21	This work
Rh_{10} *R*	6.66 (4.46 per atom)	1.21	This work
Rh_4Pd_6	6.0	1.02	This work

[a] h: hollow site (3-fold); t: on top of surface O atoms (1-fold); b: bridge between two O atoms (2-fold). [b] Bader charge in the unit of e. [c] From Ref. [63]. [d] From Ref. [23]. [e] From Ref. [64]. [f] From Ref. [65]. [g] From Ref. [66]. For M_{10} clusters the charge is for the total clsuter.

Physical Chemistry Chemical Physics Accepted Manuscript

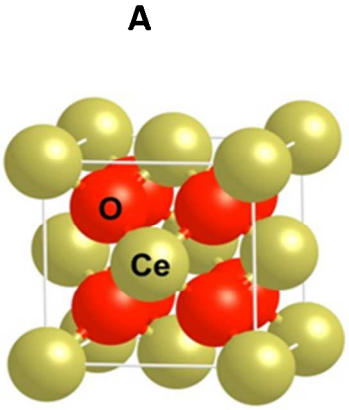

Computed surface energies (J/m^2) of CeO_2(100), (110), and (111).

Plane	Unrelaxed				relaxed			
	this work	GGA+U[b]	GGA [c]	GGA [d]	this work	GGA+U[b]	GGA [c]	GGA [d]
(100)[a]	4.15	-	-	1.98	3.68	-	-	1.43
(110)	1.29	1.17	1.25	1.19	1.06	0.96	1.05	1.01
(111)	0.60	0.61	0.69	0.61	0.59	0.60	0.68	0.60

[a]An oxygen-terminated surface was used.
[b] [67]; [c] [68]; [d] [53]

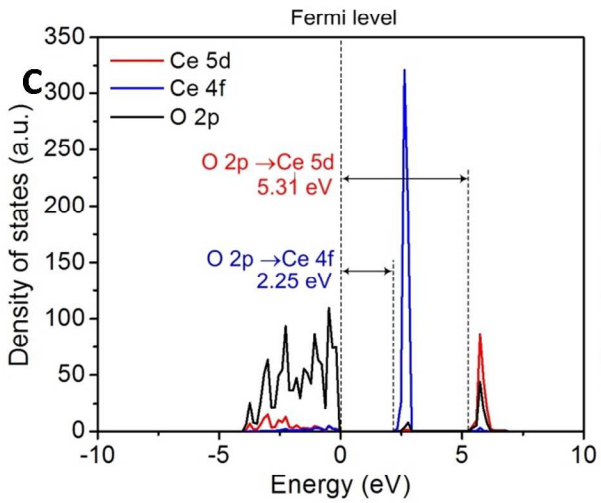

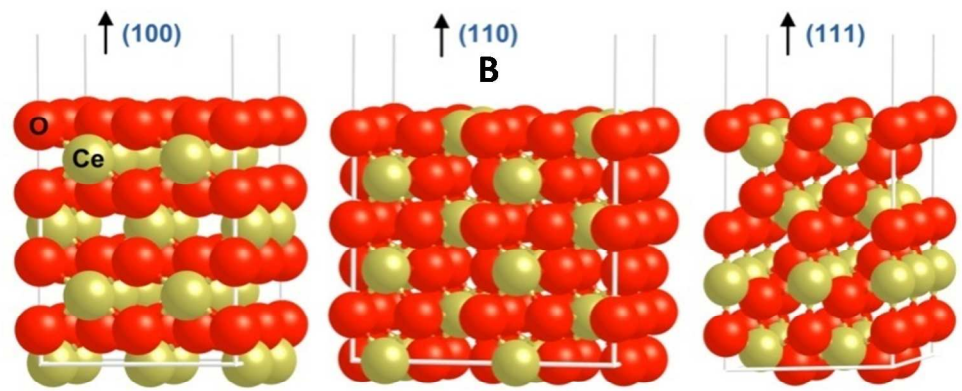

Figure 1. (a) Schematic of the fluorite structure of bulk CeO_2. (b) Total projected density of states of bulk CeO_2 at the PBE + U with U_{eff} = 5.0 eV. The energy gaps are shown in the figure. (c) Side view of slab models for CeO_2(100), (110), (111) surfaces.

Physical Chemistry Chemical Physics Accepted Manuscript

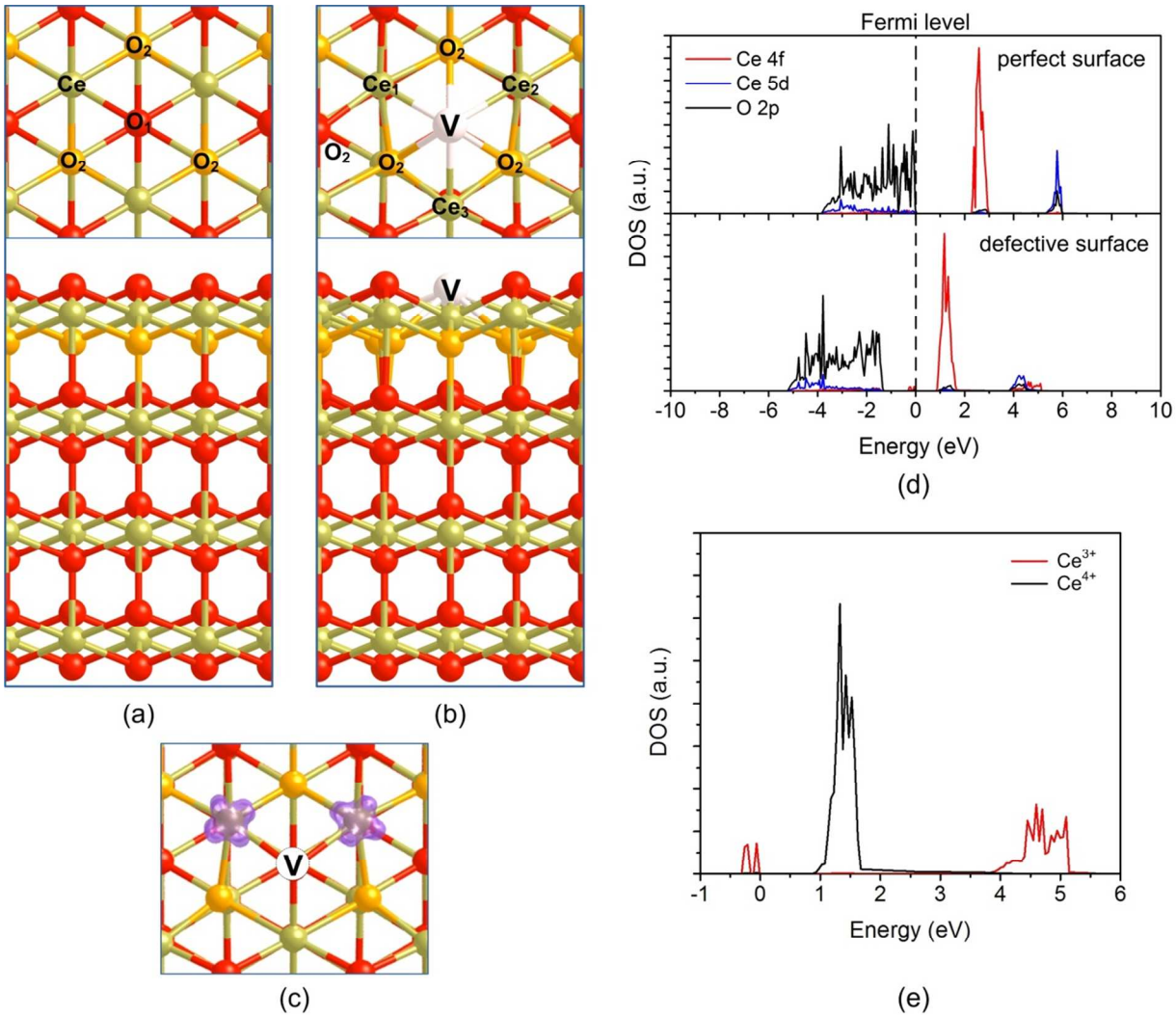

Figure 2. Top and side views of the (a) perfect and (b) defective $CeO_2(111)$ surfaces. (c) Isosurfaces of spin density for the defective CeO_2 (111) surface. The isosurfaces of the spin density plots are 0.2 electrons/Å^3, "V" is the O vacancy. For clarity, the third O layer from the top is shown in gold. (d) DOS plots of perfect (top) and defective (bottom) $CeO_2(111)$ surfaces. An oxygen vacancy (V) is located on the topmost surface by removing an O atom (as shown in figure 2A). (e) PDOS plot of Ce 4f from Ce^{3+} and Ce^{4+} on defective p(2 × 2) $CeO_2(111)$.

Physical Chemistry Chemical Physics Accepted Manuscript

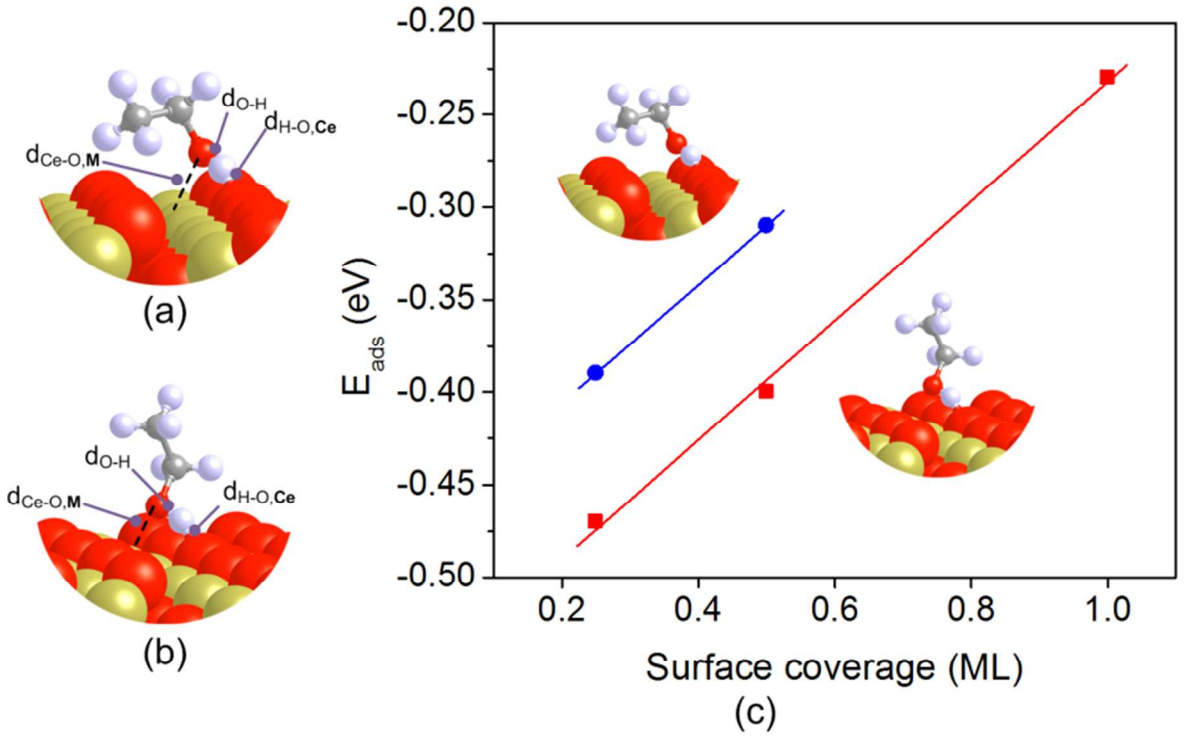

Figure 3. Schematics of adsorbed molecular ethanol species on CeO_2(111): (a) parallel and (b) vertical configurations. (c) Adsorption energies of ethanol on CeO_2 as a function of surface coverage.

Physical Chemistry Chemical Physics Accepted Manuscript

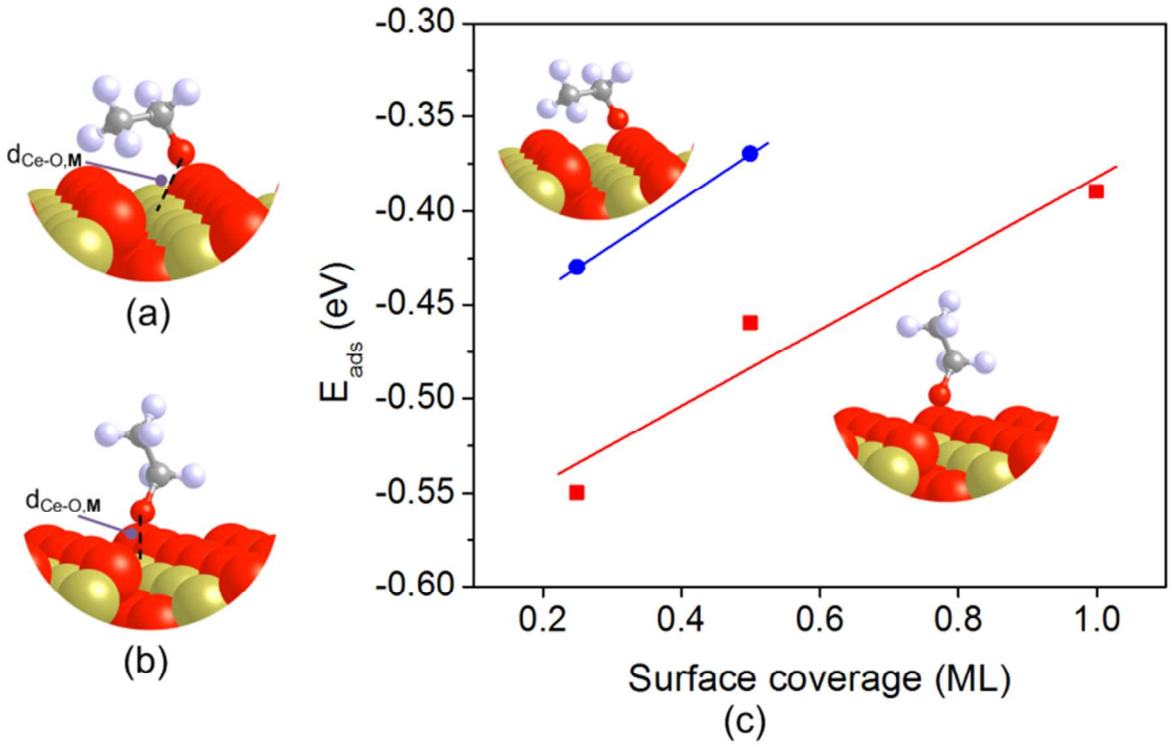

Figure 4. Schematics of adsorbed ethoxide species on CeO_2(111): (a) parallel and (b) vertical configurations. (c) Adsorption energies of ethoxide on CeO_2 as a function of surface coverage.

Physical Chemistry Chemical Physics Accepted Manuscript

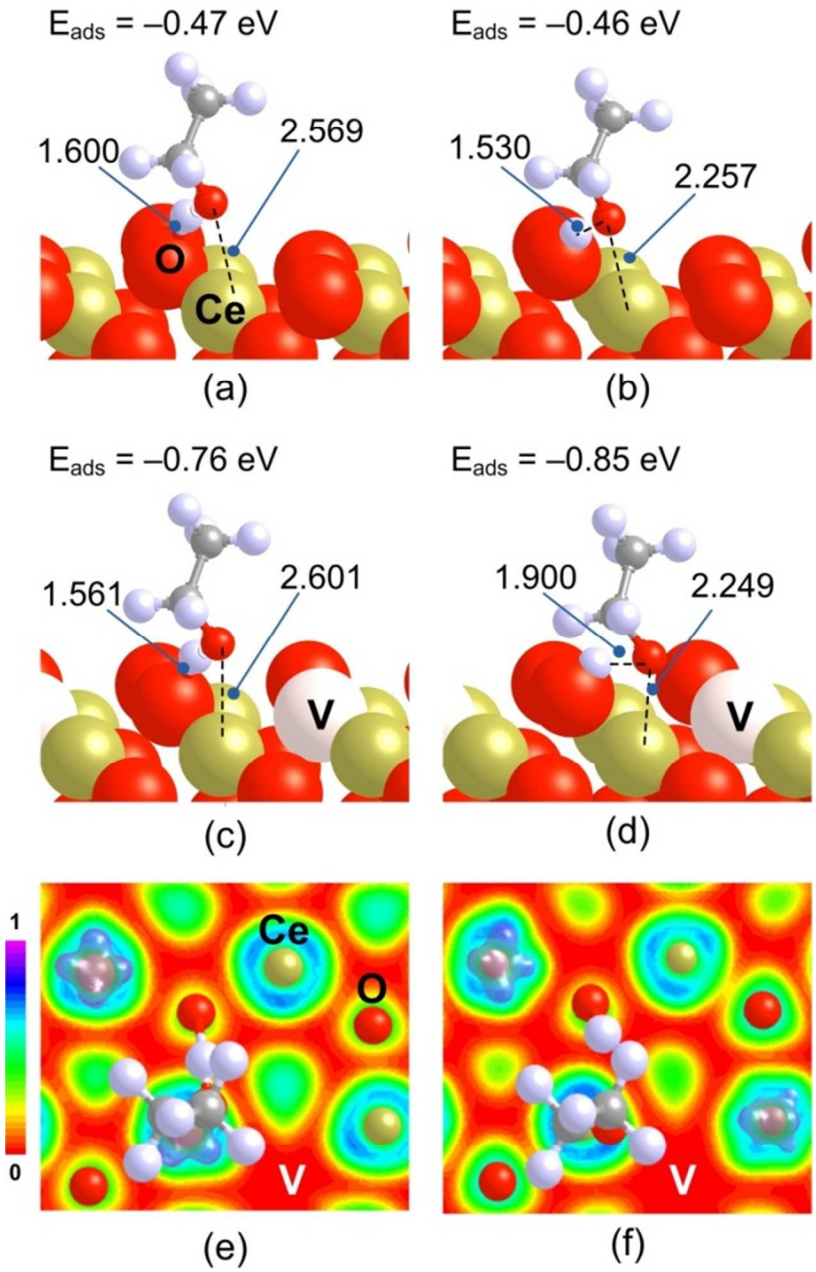

Figure 5. Geometrical illustration and adsorption energies of molecularly and dissociatively adsorbed ethanol on (a) and (b) the perfect and (c) and (d) defective p(2 × 2) CeO_2(111) surfaces with the vertical configuration. An oxygen vacancy (V) is located on the topmost surface by removing an oxygen atom. (e) and (f) Top views of Electron Localization Function (ELF) calculations for molecularly and dissociatively adsorbed ethanol on the defective surface, showing two localized Ce^{3+} ions on each surface. The isosurfaces of the spin density plots are 0.2 electrons/$Å^3$. In (e) and (f) grey balls for C, white balls for H.

Physical Chemistry Chemical Physics Accepted Manuscript

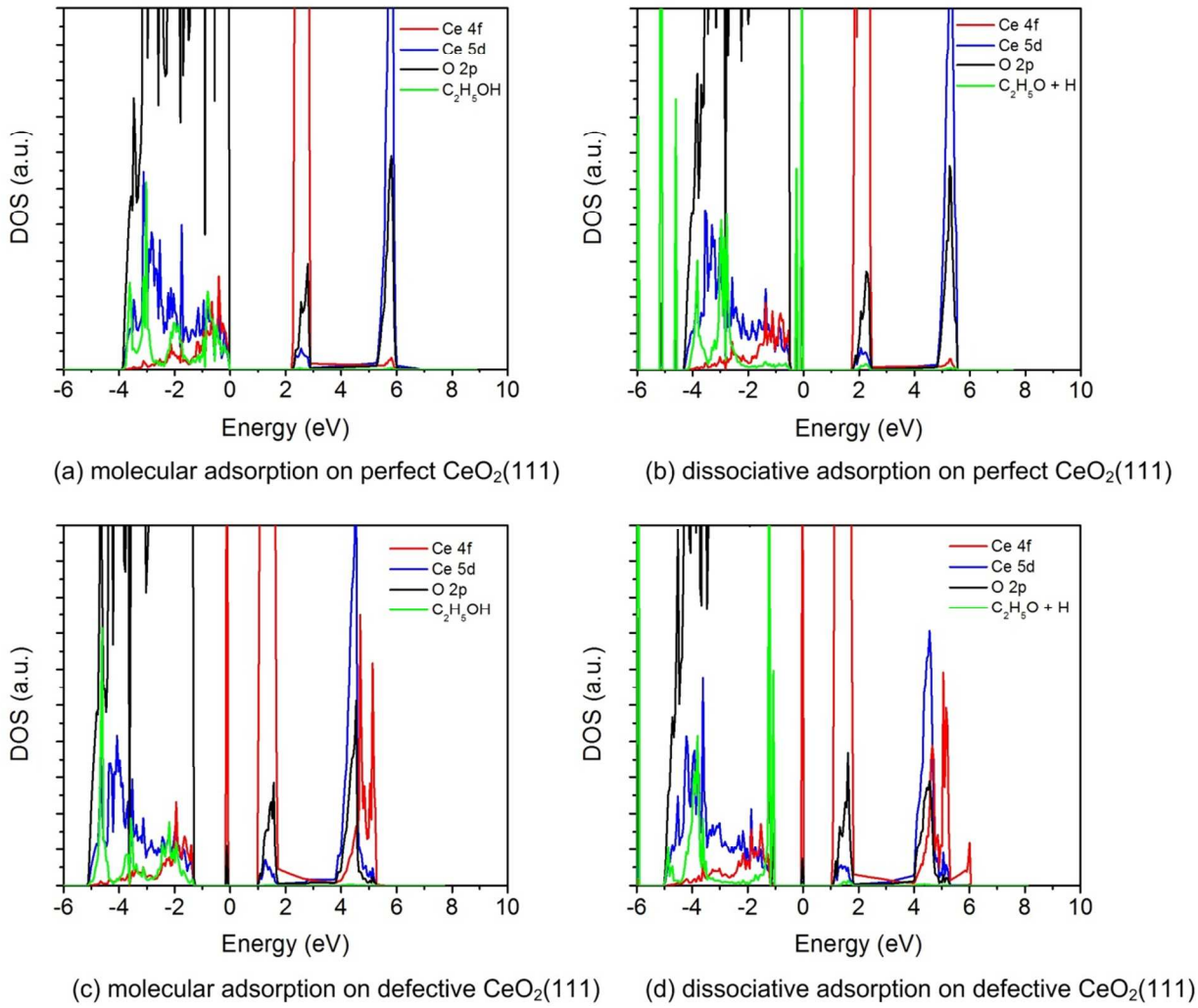

Figure 6. DOS plots of molecular and dissociative adsorptions of ethanol on the perfect and defective p(2 × 2) CeO_2(111) surfaces.

Physical Chemistry Chemical Physics Accepted Manuscript

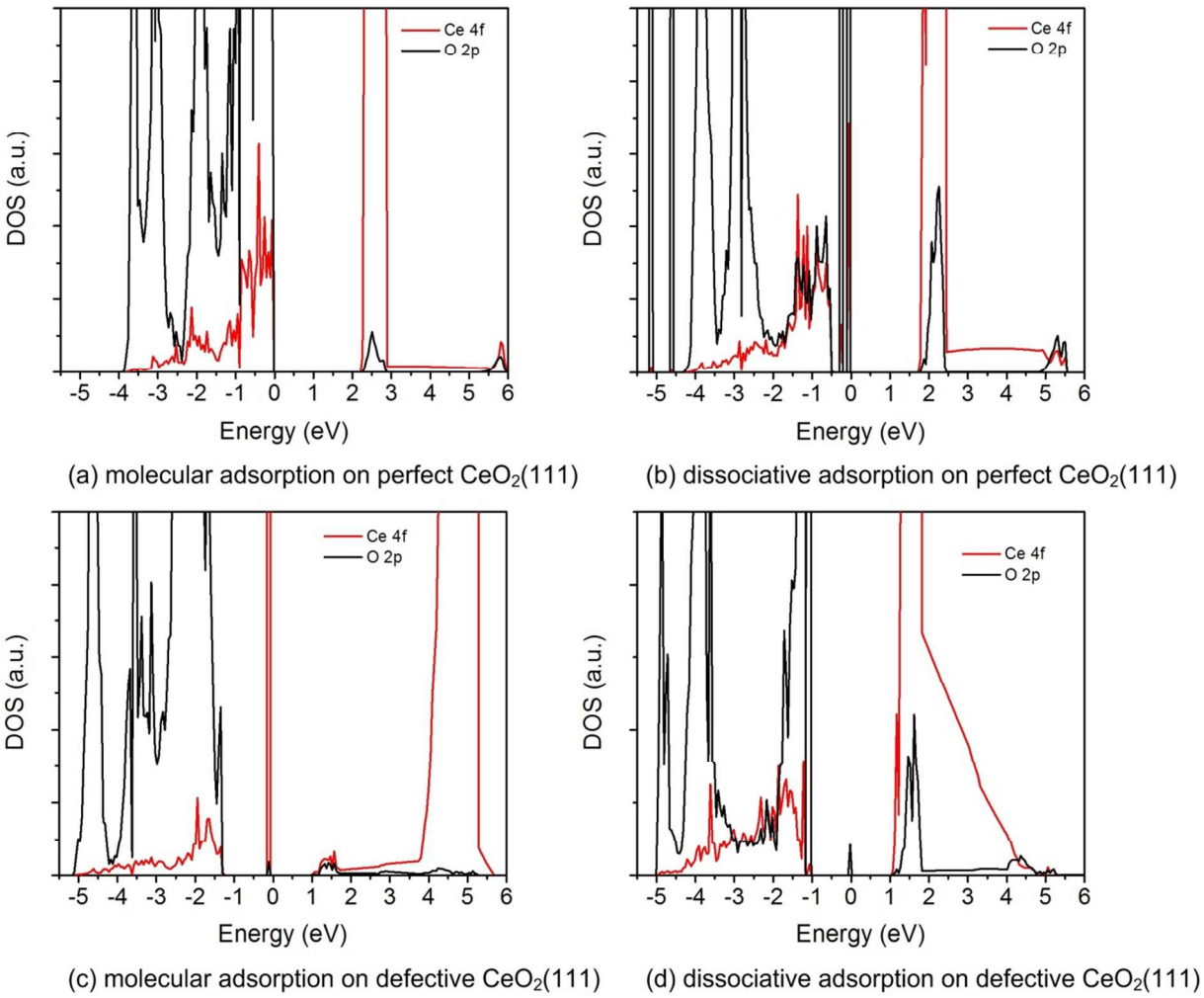

Figure 7. DOS plots of O and Ce atoms involved in the bonding for the molecular and dissociative adsorptions of ethanol on the perfect and defective p(2 × 2) CeO_2(111) surfaces.

Physical Chemistry Chemical Physics Accepted Manuscript

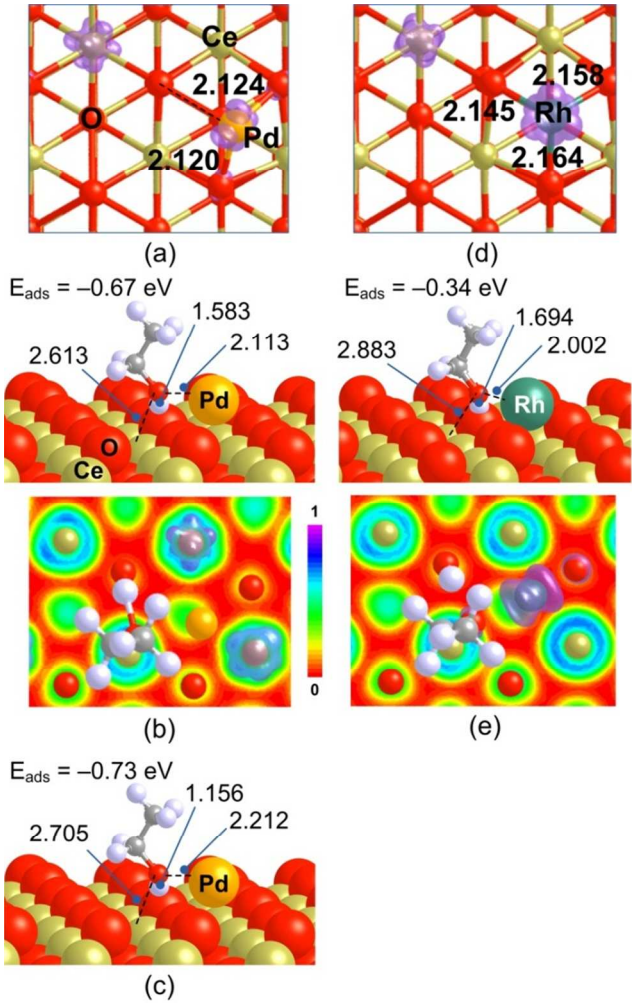

Figure 8. (a) Pd adsorption on perfect $CeO_2(111)$. (b) Dissociative adsorption of ethanol on $Pd/CeO_2(111)$ and its ELF contour plot. (c) Molecular adsorption of ethanol on $Pd/CeO_2(111)$. (d) Rh adsorption on $CeO_2(111)$. (e) Dissociative adsorption of ethanol on $Rh/CeO_2(111)$ and its ELF contour plot. The isosurfaces of the spin density plots are 0.2 electrons/$Å^3$. In (b) and (e) red balls for O, large golden for Pd, large dark blue for Rh, small golden for Ce, white for H and grey for C.

Physical Chemistry Chemical Physics Accepted Manuscript

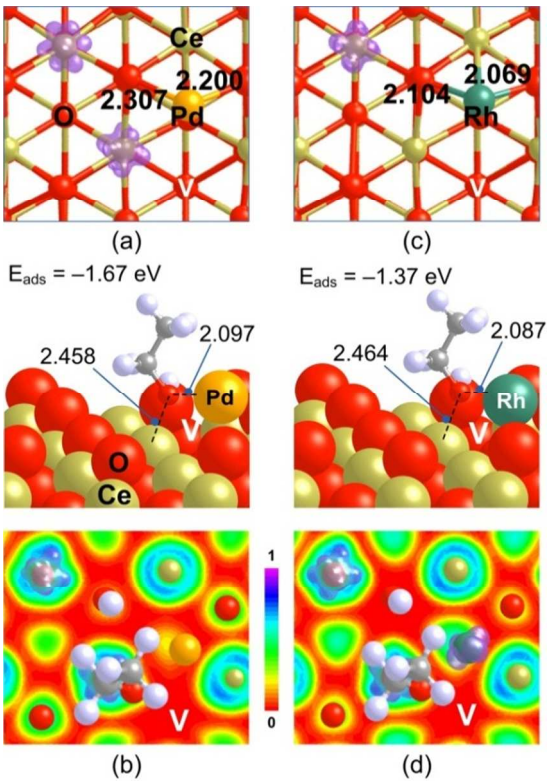

Figure 9. (a) Pd adsorption on defective CeO_2(111). (b) Dissociative adsorption of ethanol on the defective Pd/CeO_2(111) and its ELF contour plot. (c) Rh adsorption on defective CeO_2(111). (d) Dissociative adsorption of ethanol on defective Rh/CeO_2(111) and its ELF contour plot. The isosurfaces of the spin density plots are 0.2 electrons/$Å^3$, "V" is an oxygen vacancy. In (b) and (d) red balls for O, large golden for Pd, large dark blue for Rh, small golden for Ce, white for H and grey for C.

Physical Chemistry Chemical Physics Accepted Manuscript

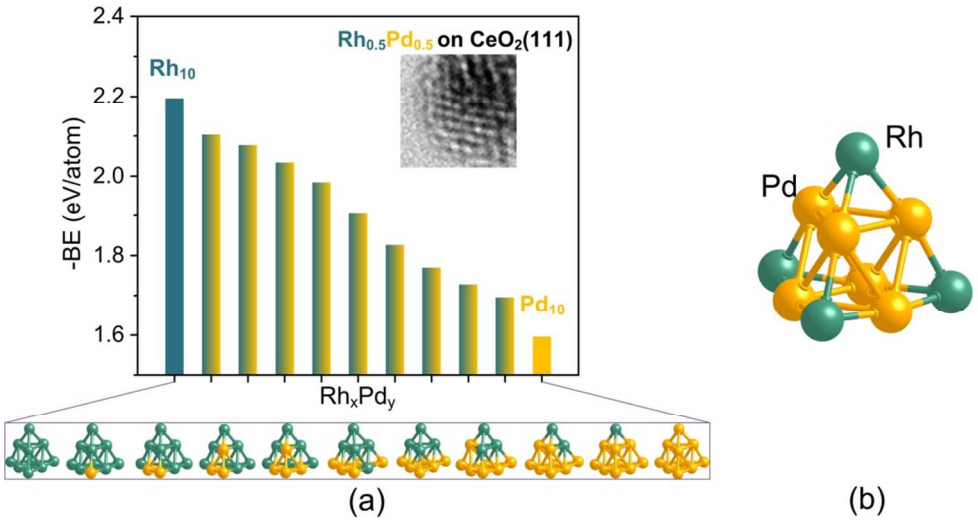

Figure 10. (a) Comparison of gas-phase Rh_xPd_y nanoclusters (x + y = 10) against the binding energy (BE) in eV/atom. (b) Optimized structure of the C_{3V} Rh_4Pd_6 nanocluster.

Physical Chemistry Chemical Physics Accepted Manuscript

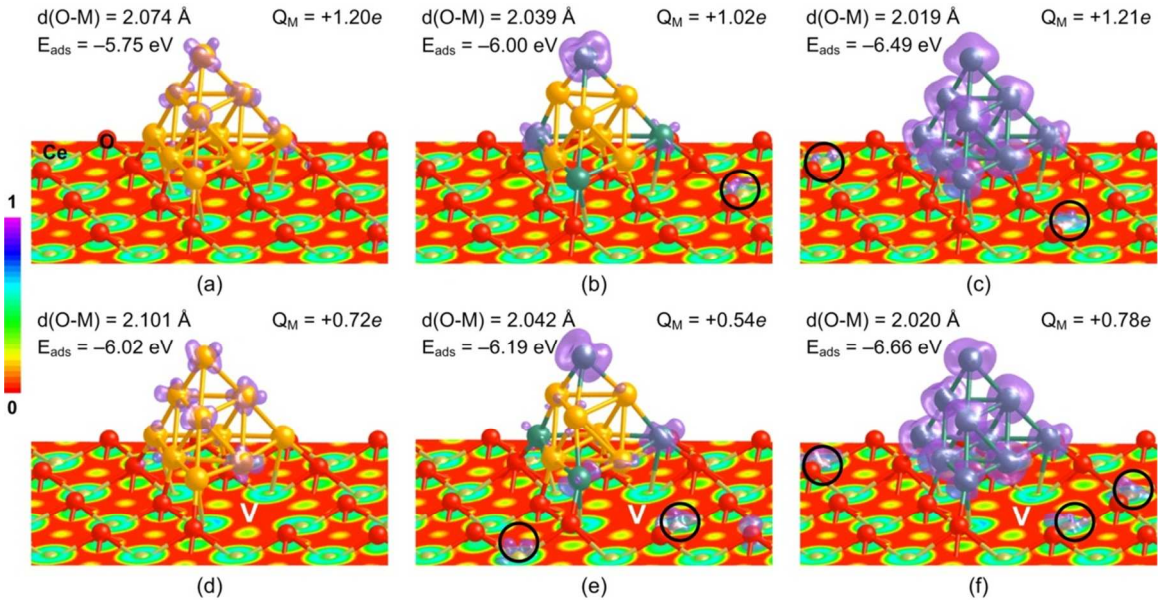

Figure 11. Adsorption of (a) Pd_{10}, (b) Rh_4Pd_6, and (c) Rh_{10} nanoclusters on perfect $CeO_2(111)$ and of (d) Pd_{10}, (e)) Rh_4Pd_6, and (f) Rh_{10} nanoclusters on defective $CeO_2(111)$. "V" represents an oxygen vacancy. The isosurfaces of the spin density plots are 0.1 electrons/$Å^3$. Rh and Pd atoms are dark blue and golden colors respectively.

Physical Chemistry Chemical Physics Accepted Manuscript